Supporting Information

Dual-function antibacterial micelle *via* self-assembling block copolymers with various antibacterial nanoparticles

Qing Zhong,[1,†] Hui Long,[1] Wei Hu,[1,†] Liujun Shi,[1] Fei Zan,[3] Meng Xiao,[1] Shaozao Tan,[1] Yu Ke,[2,*] Gang Wu[3,*] and Huifang Chen[4,*]

[1]Guangdong Engineering & Technology Research Centre of Graphene-Like Materials and Products, College of Chemistry and Materials Science, Jinan University, Guangzhou 510632, China

[2]Department of Biomedical Engineering, Key Laboratory of Biomaterials of Guangdong Higher Education Institutes, College of Life Science and Technology, Jinan University, Guangzhou 510632, China

[3]Department of Biomedical Engineering, South China University of Technology, Guangzhou 510641, China

[4]College of pharmacy, Guangdong Lingnan Institute of Technology, Guangzhou,510663, China

[†]These authors contribute equally.

*Corresponding author, E-mail addresses: lisa6863@163.com (Y. Ke), imwugang@scut.edu.cn (G. Wu), chenhf_1968@163.com (H. Chen).

Results and discussion

FTIR spectra

FTIR analysis of ZnO NPs and Ag-ZnO NPs is illustrated in Figure S1. The stretching bands in 400 ~ 600 cm^{-1} were the typical absorption peaks of ZnO NPs (Figure S1, I-a), in which the sharp peaks at 431.1 cm^{-1} and 520.5 cm^{-1} were attributed to the lattice vibration of ZnO. The broad peak at 3660.2 cm^{-1} was assigned to the vibration of the hydroxyl on the surface of ZnO NPs. Two distinct peaks at 1387.6 cm^{-1} and 1506.7 cm^{-1} corresponded to the bending vibration of CO_3^{2-},[1] perhaps owing to the reaction of sodium hydroxide and air during the synthesis of ZnO NPs.

Figure S1 (I-b) indicates the FTIR spectrum of Ag-ZnO NPs. The bands at 3430.8 cm^{-1} and 1611.9 cm^{-1} were attributed to the stretching and bending vibration of the hydroxyl groups on Ag-ZnO surface. The absorption bands at 2924.4 $cm^{-1}$and 1391.1 cm^{-1} belonged to the stretching vibration of N-O in nitrate. The peaks at 794.1 cm^{-1} and 704.7 cm^{-1} were assigned to the stretching vibration of Zn-O-H and the bending vibration of Zn-O-Zn, respectively. An additional peak at 627.0 cm^{-1} was perhaps due to the formation of Ag-ZnO NPs. Compared with those of ZnO NPs, the characteristic stretching vibration of Zn-O in 400 ~ 600 cm^{-1} shifted to lower values because the electron cloud density of Zn-O decreased *via* the inductive effect of Ag. Additionally, the sharp peaks at 1506.7 cm^{-1} and 1387.6 cm^{-1} in the FTIR spectrum of ZnO NPs disappeared.

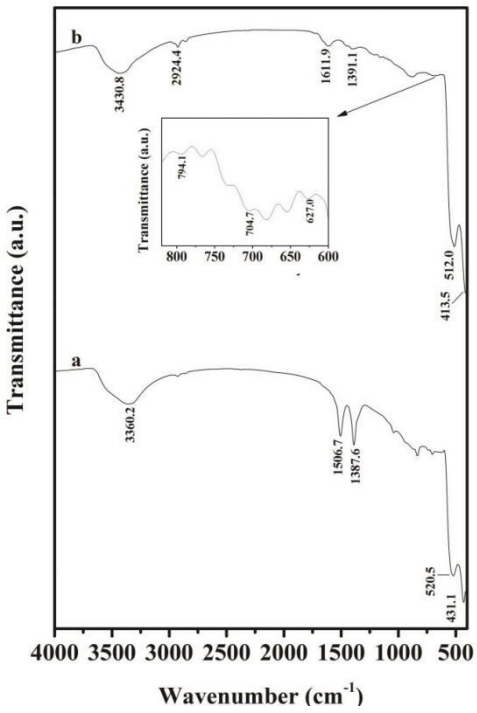

Figure S1. FTIR spectra of the nanocomposites of ZnO NPs (a) and Ag-ZnO NPs (b)

XRD spectra

XRD patterns of ZnO and Ag-ZnO NPs is shown in Figure S2. Ag-ZnO NPs presented the distinctive diffraction peaks at 32.1°, 34.7°, 36.6°, 47.9°, 56.9°, 63.2°, 66.6°, 68.3°, 69.4°, 72.8° and 77.3°, corresponding to (100), (022), (101), (102), (110), (103), (200), (112), (201), (004) and (202) planes of hexagonal (wurtzite) crystal structure of ZnO NPs, respectively. Another peaks at 2θ = 38.4°, 44.6° and 64.9° of Ag-ZnO NPs matched with the (111), (200) and (220) planes of metallic silver. Compared with ZnO, the diffraction position and lattice parameters of Ag-ZnO did not change remarkably, indicating that Ag was not doped into ZnO lattice. This can be attributed to a larger silver ion radius ($r_{(Ag^{+})}$=126pm) than the zinc ion radius ($r_{(Zn^{2+})}$ = 74pm), therefore, the silver metalloid phase was formed on the surface of ZnO NPs. The crystallite size and interplanar spacing of naroparticles were

calculated by Bragg equation ($2d\sin\theta = n\lambda$) and Scherer's formula ($D=0.9\lambda/\beta \cos\theta$). The crystal spacing (d) and particle size (D) were 2.45 Å and ~45.51 nm for ZnO NPs, and 2.34 Å and ~41.77 nm for Ag metallic NPs, respectively.

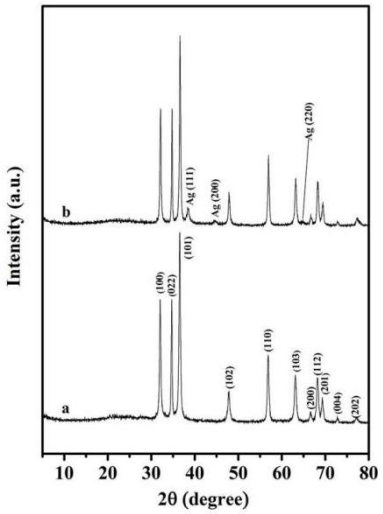

Figure S2. XRD spectra of ZnO (a) and Ag-ZnO (b) NPs

Thermal decomposition

Figure S3 illustrates TGA and DTG plots of PPP_{312}-ZnO and PPP_{312}-Ag-ZnO with different contents of the nanoparticles, and the corresponding parameters are summarized in Table S1. Similar to PPP_{312}, the nanocomposites presented two major degradation stages caused by the thermal decomposition of PHBV and PEG successively. The initial and final decomposition temperatures and the peak decomposition temperature (T_i, T_f and T_p) of the nanocomposites reduced compared with those of PPP_{312}, by (13.3~22.4) °C, (9.8~17.5) °C, (10.3~16.7) °C and (7.4~18.3) °C, (2.0~7.7) °C, (11.9~17.4) °C, respectively for the first and second main stages, indicating the influence of the nanoparticles on the thermal degradation of the triblock copolymers.

In the first main stage, the nanocomposites with 10% NPs showed a weigh loss of about 34.8% between 243.5 °C and 278.6 °C, while a weight loss of 41.1~42.5% for the nanocomposites with 5% NPs was observed within 252.2~285.4 °C; As the content of the nanoparticles increased, T_{i1}, T_{f1}, T_{p1} and the weight loss (W_1) reduced significantly. ZnO and Ag-ZnO NPs would weaken PHBV-PEG interaction and

promote the oxidative decomposition of PPP_{312}. The carboxyl groups *via* the thermal degradation of PHBV (PHB) may react with hydroxyl groups of the decomposed PEG segments, instead of the hydroxyl groups on ZnO surface. The later case may form carboxylate-zinc oxide compounds to improve the thermal stability of PHB/ZnO composites[2]. In the second stage, the nanocomposite with 10% NPs decomposed with a weight loss of 24.9~27.4% within 355.5~417.5 °C, and a weight loss of 24.6~25.4% within 353.7~418.4 °C for that of 5% NPs. The effect of nanoparticles on the thermal degradation of PEG fragments was not obvious, and silver had little effect on the thermal properties of the nanocomposites.

While subtracting the residual weight of PPP_{312} (~7.49%), the residual contents at 800 °C were 7.98%, 4.40%, 8.01% and 5.88%, respectively for PPP_{312}-10% Ag-ZnO, PPP_{312}-5% Ag-ZnO, PPP_{312}-10% ZnO and PPP_{312}-5% ZnO, which would be the weight percentage of ZnO or Ag-ZnO NPs because the nanocomposites did not lose weight remarkably at temperatures above 500 °C. These contents were little smaller than the theoretical ones, perhaps owing to volatilization of water or small molecules that had been physically adsorbed on the nanoparticles surface below 250 °C.

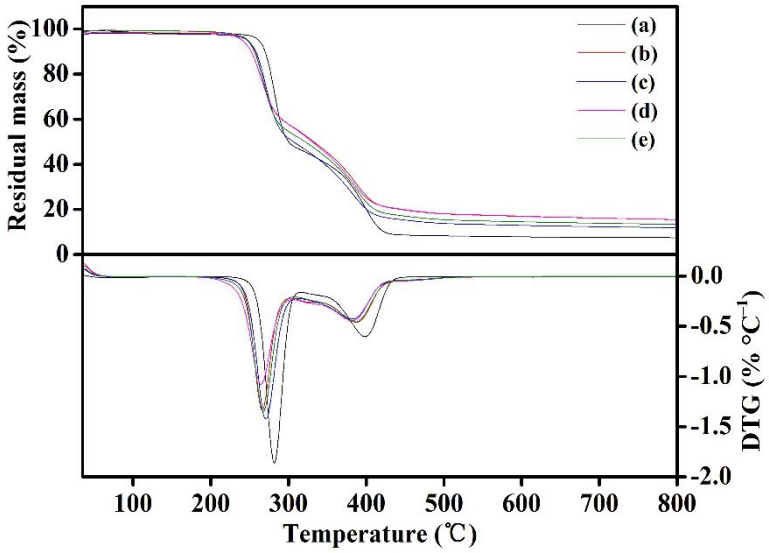

Figure S3. TGA and DTG curves of PPP_{312} (a), PPP_{312}-10% Ag-ZnO (b), PPP_{312}-5%

Ag-ZnO (c), PPP_{312}-10% ZnO (d), PPP_{312}-5% ZnO (e)

Table S1. Thermal degradation properties of PPP_{312}-Ag-ZnO and PPP_{312}-ZnO nanocomposites

Sample	T_{i1} (°C)[a]	T_{f1} (°C)[b]	T_{p1}(°C)[c]	W_1 (%)[d]	T_{i2} (°C)[a]	T_{f2} (°C)[b]	T_{p2}(°C)[c]	W_2 (%)[d]	CR (%)[e]
PPP_{312}	265.9	295.2	281.4	46.32	372.0	420.4	399.8	26.61	7.49
PPP_{312}-10% Ag-ZnO	249.5	277.7	266.1	34.74	364.6	417.5	387.3	27.35	15.47
PPP_{312}-5% Ag-ZnO	252.6	285.4	271.1	42.46	353.7	412.7	383.9	24.57	11.89
PPP_{312}-10% ZnO	243.5	278.6	264.7	34.76	355.5	414.7	382.7	24.87	15.50
PPP_{312}-5% ZnO	252.2	283.8	267.5	41.07	357.7	418.4	387.9	25.40	13.37

[a]: T_{i1} and T_{i2} representing the initial thermal degradation temperatures of the first and second main degradation process, respectively.
[b]: T_{f1} and T_{f2} representing the final thermal degradation temperatures of the first and second main degradation process, respectively.
[c]: T_{p1} and T_{p2} representing the peak temperatures that correspond to the maximum degradation rate in the first and second main degradation process, respectively.
[d]: W_1 and W_2 representing the mass loss percentages of the first and second main degradation process, respectively.
[e]: CR representing char residue at 800 °C.

Reference:

1. Shah, J.; Kotnala, R. K., Rapid green synthesis of ZnO nanoparticles using a hydroelectric cell without an electrolyte. *Journal of Physics and Chemistry of Solids* **2017,** *108*, 15-20.
2. Rodríguez-Tobías, H.; Morales, G.; Ledezma, A.; Romero, J.; Saldívar, R.; Langlois, V.; Renard, E.; Grande, D., Electrospinning and electrospraying techniques for designing novel antibacterial poly (3-hydroxybutyrate)/zinc oxide nanofibrous composites. *Journal of Materials Science* **2016,** *51* (18), 8593-8609.